land

MDPI

Article

Comprehensive Comparative Analysis and Innovative Exploration of Green View Index Calculation Methods

Dongmin Yin [1] and Terumitsu Hirata [2,*]

[1] Department of Urban and Civil Engineering, Graduate School of Science and Engineering, Ibaraki University, Hitachi 316-8511, Japan; 22nd313y@vc.ibaraki.ac.jp
[2] Department of Urban and Civil Engineering, Faculty of Applied Science and Engineering, Ibaraki University, Hitachi 316-8511, Japan
* Correspondence: terumitsu.hirata.a@vc.ibaraki.ac.jp; Tel.: +81-(0)294-38-5326

Abstract: Despite the widespread use of street view imagery for Green View Index (GVI) analyses, variations in sampling methodologies across studies and the potential impact of these differences on the results, including associated errors, remain largely unexplored. This study aims to investigate the effectiveness of various GVI calculation methods, with a focus on analyzing the impact of sampling point selection and coverage angles on GVI results. Through a systematic review of the extensive relevant literature, we synthesized six predominant sampling methods: the four-quadrant view method, six-quadrant view method, eighteen-quadrant view method, panoramic view method, fisheye view method and pedestrian view method. We further evaluated the strengths and weaknesses of each approach, along with their applicability across different research domains. In addition, to address the limitations of existing methods in specific contexts, we developed a novel sampling technique based on three 120° street view images and experimentally validated its feasibility and accuracy. The results demonstrate the method's high reliability, making it a valuable tool for acquiring and analyzing street view images. Our findings demonstrate that the choice of sampling method significantly influences GVI calculations, underscoring the necessity for researchers to select the optimal approach based on a specific research context. To mitigate errors arising from initial sampling angles, this study introduces a novel concept, the "Green View Circle", which enhances the precision and applicability of calculations through the meticulous segmentation of observational angles, particularly in complex urban environments.

Keywords: Green View Index; street view images; sampling methods; perspective coverage; Green View Circle; urban greening

Academic Editor: Thomas Panagopoulos

Received: 17 December 2024
Revised: 26 January 2025
Accepted: 28 January 2025
Published: 30 January 2025

Citation: Yin, D.; Hirata, T. Comprehensive Comparative Analysis and Innovative Exploration of Green View Index Calculation Methods. *Land* **2025**, *14*, 289. https://doi.org/10.3390/land14020289

1. Introduction

The Green View Index (GVI), a metric for assessing the extent of urban greening, was first referred to by Japanese scholar Yoji Aoki in 1987 [1]. GVI is defined as the ratio of the vegetation area within the human visual field to the total area of the human visual field. Given the complexity of defining human vision, the index is directly represented as the percentage of green vegetation in street view images or images of a particular location [2]. This index not only reflects public perception and satisfaction with urban greening through visual assessment, but also highlights the significant impact of large trees and their distribution on the extent of urban greening [3]. Furthermore, it effectively quantifies visual greening along roadways, providing valuable insights for urban green space planning and management [3,4].

The GVI has applications in various domains, including urban green spaces and health [5], urban planning and design [6], ecosystem services [7], socioeconomic impacts [8], sustainable transportation [9], climate adaptability [10], landscape esthetics and culture [11], and environmental justice [12]. There are two primary methods for obtaining GVI images: manual field collection and collection via street view maps. The latter method offers significant savings in terms of both labor and resources compared to the former.

A review of 70 recent studies utilizing street view images for GVI analysis indicates diverse methods for sampling street view images [10,13–17]. These methods, which were developed through extensive exploration by previous researchers, highlight the direct impact of different street view collection methods on GVI calculations. Researchers are often aware of and attempt to avoid errors arising from various GVI calculation methods. However, there has been no systematic review or horizontal comparison of the existing collection methods. This study aims to compare various existing methods of obtaining street view images from different perspectives and to analyze their impact on GVI computation. In addition, a novel image sampling method for GVI was proposed and its reliability was validated, with the objective of enhancing the accuracy and applicability of GVI calculations. Building on a comprehensive analysis of five primary sampling methods, this study introduces a novel concept, "Green View Circle", (GVC) to improve the precision of GVI measurements through finer angular segmentation.

2. Literature Review

2.1. Exploring the Concept of GVI

The term "view" is defined in the Cambridge Dictionary as "what you can see from a particular place" [18]. Visual perception is determined by the human eye, which converts light into neural signals that are transmitted to the brain [19]. In essence, the scenes we observe result from the processing of visual information by the brain [20].

As early as in the seventeenth century, optical scientists discovered that the visual information humans receive is inherently two-dimensional [21,22]. Our ability to perceive a three-dimensional world arises from our extensive visual experience, enabling us to make instantaneous judgments and construct a three-dimensional representation from two-dimensional visual input [23].

Based on this understanding, what exactly are we discussing when we refer to the "GVI"?

If the GVI is defined as the proportion of green within the human visual field, human visual perception should be simulated as closely as possible when obtaining the GVI from street view images [4]. However, the human visual field is limited and, at any given moment, cannot fully capture all "green" information within its range. The GVI is typically used to comprehensively assess street greening from a human perspective. To calculate the index, it is thus assumed that all green information present within the visual field can be comprehensively captured by simulating a 360° panoramic view of the human eye [24]. This represents the underlying logic of acquiring the GVI from street view images.

Street view imagery serves as a vital data source when calculating the GVI, as it closely replicates the human visual perspective by capturing urban greenery within the visible field [25]. This method provides a high-resolution and realistic approach to assess urban greening and effectively simulate human perception of greenery in urban environments [26–28].

2.2. Current Status of the GVI Planning and Application

In 2004, the Japanese government enacted the "Three Laws of Scenic Green", using the GVI to evaluate and enhance urban greening levels [29]. In 2010, Kyoto introduced

the "Basic Plan for Green Spaces", incorporating the GVI in its greening goals [30]. By 2012, Osaka revised its "New Basic Plan for Green Spaces", adding the GVI to its greening indicators, selecting eight critical urban nodes for regular GVI surveys, and publishing the results as a key measure of urban greening progress [31]. In March 2018, Tokyo's "Shinjuku Ward Basic Plan for Green Spaces (Revised)" introduced the concept of the GVI and proposed four primary enhancement directions: collaborative urban greening, creating visible greenery, increasing biodiversity, and preserving and enriching parks. The goal of "creating visible greenery" is to improve the greenery that is visible to residents in public open spaces [32].

Over the past two decades, various local governments in Japan have adopted the GVI as a crucial evaluation metric in urban greening planning. However, they primarily rely on on-site photography for street view acquisition, rather than employing online street view images. For example, in Osaka, cameras were positioned at a height of 1.5 m to capture images from various angles and locations, such as three street views from a pedestrian path (front, rear, and facing the main road), two street views from the center of roads without pedestrian paths (front and rear), one street view from the center of a bridge (river-facing), four street views from each corner of intersections (toward the center), and three street views from the entrances of terminal buildings (left, right, and front). Detailed GVI calculation methods have contributed to the refinement of urban management.

In Beijing, China, the "Regulatory Detailed Planning for Core Functional Areas (Block Level) (2018–2035)" guideline explicitly states the need to build a universally shared green space system, enhance three-dimensional greening effects, and improve the GVI levels [33]. The "Technical Specifications for Ecological Environment Quality Evaluation", released in 2021, includes the GVI as an indicator for assessing the ecological environment quality of urban built-up areas, with a weight of 0.1 in the calculation of the vegetation coverage index [34]. Guangzhou's "Green Space System Plan (2021–2035)" also employs the GVI as a metric for evaluating transportation hubs and historical districts, with targets set for GVI levels to exceed 35% and 25%, respectively, by 2035 [35]. Shenzhen's "Overall Plan for Park City Construction and Three-Year Action Plan (2022–2024) (Draft)", issued on May 28, 2022, outlines the comprehensive development of vertical greening and the enhancement of urban GVI and visual esthetics [36].

To address urban green space equity issues, the "Seoul 2030 Plan" emphasizes the need for fair green space usage [37]. To accurately assess the inequality of green space distribution in Seoul, local researchers employed Google Street View (GSV) and computer vision techniques to generate current GVI distribution maps for administrative districts, determining the degree of green space inequality in each district [38,39].

The Senseable City Lab of the Massachusetts Institute of Technology (MIT), in collaboration with the World Economic Forum, created Treepedia, an interactive website that shows green density maps of major cities worldwide. The site indicates that Tampa, Florida, has the highest average GVI of 36.1% [40].

3. Overview of Sampling Methods

3.1. Overview of Existing Sampling Methods and Applications

After a comprehensive analysis of the literature, we categorized street view image acquisition methods into several types, as follows:

A. Four-quadrant view method

This method divides a 360° street view into four 90° segments, calculates the GVI for each segment, and then averages the results. The formula is as follows:

$$GVI = \frac{Area_{g\_i}}{Area_{t\_i}} \times 100\% = \frac{\sum GVI_i}{i}(i = 4), \quad (1)$$

where the GVI is the Green View Index, $Area_{g\_i}$ indicates the green area in the i-th image, and $Area_{t\_i}$ denotes the total area in the i-th image.

The four-quadrant view method schematic diagram is shown in Figure 1.

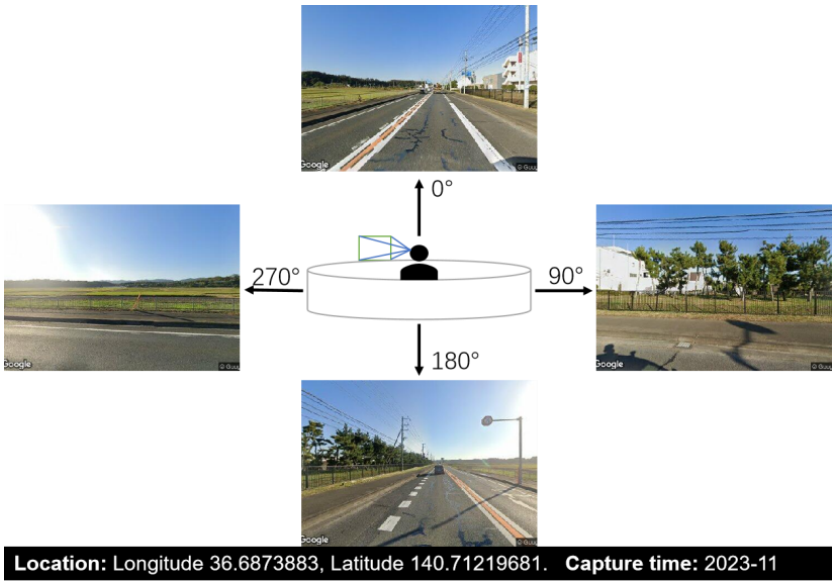

Figure 1. Schematic depicting the four-quadrant view method (data source: Google Street View).

This approach has been widely used in various studies of GVI applications. For instance, it has been used in research analyzing the impact of urban street greening on factors such as childhood asthma, obesity, diabetes, lung function, and other metabolic syndromes [41–45]. It has also been used in combination with the Normalized Difference Vegetation Index (NDVI) for the spatial analysis of urban greening [46–48], as well as in studies examining the influence of the built environment on jogging behavior using GPS trajectory data [49–51]. Additionally, it has been applied in research addressing urban environmental justice issues through socioeconomic and green space data [52,53].

This method is most commonly used in GVI calculations because of its economic efficiency and minimal average workload due to the smaller number of street view images required. Notably, this method is predominantly used when the number of sampling points exceeds 100,000. Interestingly, most researchers employing this method are from China, suggesting that researchers from the same linguistic region may adopt similar methodologies because of ease of communication, leading to methodological convergence.

B. Six-quadrant View Method

This method is another widely used sampling approach involving image stitching. It divides a 360° street view into six 60° segments, calculates the GVI for each segment, and averages the results. The calculation formula is given below:

$$GVI = \frac{Area_{g\_i}}{Area_{t\_i}} \times 100\% = \frac{\sum GVI_i}{i}(i = 6), \quad (2)$$

The six-quadrant view method schematic diagram is shown in Figure 2.

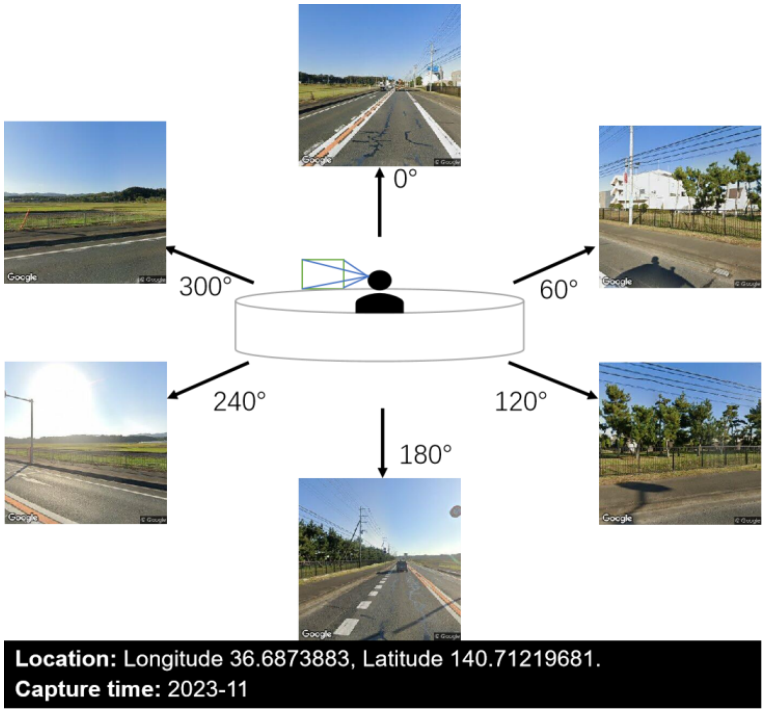

Figure 2. Schematic depicting the six-quadrant view method (data source: Google Street View).

This method has been applied across a range of research areas. For example, scholars from Osaka, Japan, studied optimal walking paths based on GVI [54], while researchers from Helsinki, Finland, evaluated perceived satisfaction with jogging routes using jogging behavior data [55]. This method was used in the Treepedia project at MIT to compile the GVI data for 34 cities [40].

Although this method approximates calculations, it reduces the distortions present in street view images compared to those present when using the four-quadrant view method, resulting in more accurate GVI measurements. However, this increases both the workload for obtaining street view images and the complexity of the computations. This method is more favored by researchers outside China than the four-quadrant view method.

C. Eighteen-quadrant View Method

In addition to the commonly used quadrant-based and six-quadrant view methods, researchers optimized the sextant-based approach to obtain a more comprehensive street view. This method adds 12 additional images at 45° upward and downward angles to the original 360° horizontal view, aiming to obtain a more comprehensive GVI calculation. The calculation formula is as follows:

$$GVI = \frac{\sum_{i=1}^{6}\sum_{v=1}^{3} Area_{g\_iv}}{\sum_{i=1}^{6}\sum_{v=1}^{3} Area_{t\_iv}} \times 100\%, \quad (3)$$

where the GVI is the Green View Index, $Area_{g\_iv}$ indicates the green area in the i-th image at elevation angle v, and $Area_{t\_iv}$ denotes the total area in the i-th image at elevation angle v.

The eighteen-quadrant view method schematic diagram is shown in Figure 3.

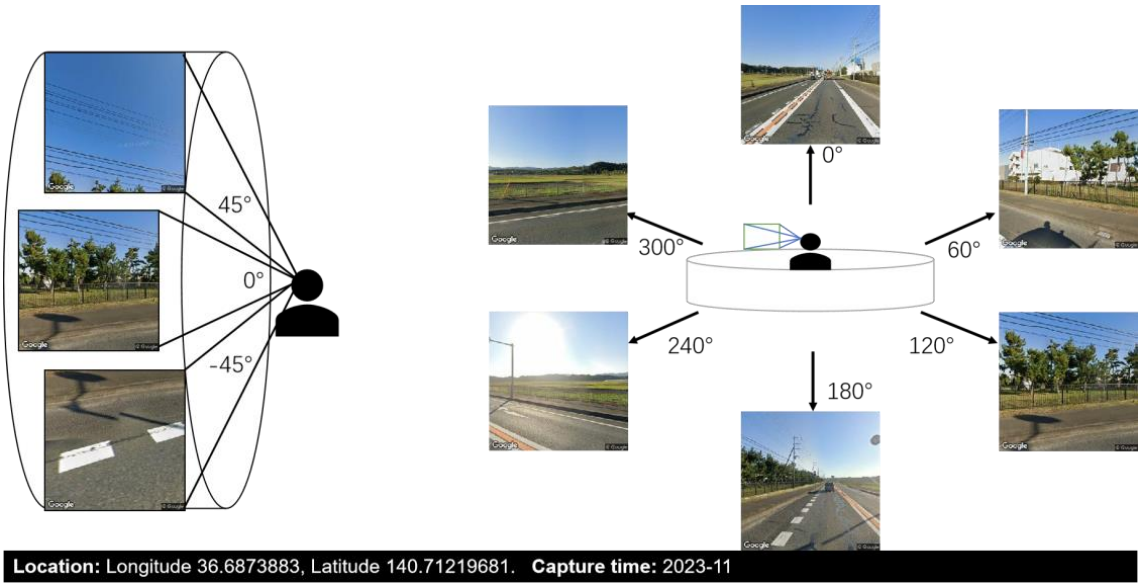

Figure 3. Schematic depicting the eighteen-quadrant view method (data source: Google Street View).

This approach is frequently used in urban planning and design. It was employed to assess urban street tree characteristics in conjunction with NDVI [56] and to evaluate the spatial distribution of buildings and green spaces [15,57]. Notably, some researchers investigating the relationship between community greening indices and air particulate matter adopted a modified twelve-quadrant view method, excluding the −45° angle images [58].

While theoretically capturing more green information, this method may result in lower GVI outcomes owing to the inclusion of a significant amount of sky and road surface information, which can dilute the actual green view.

D. Panoramic View Method

The panoramic view method involves capturing a single comprehensive 360° panoramic image to represent the visual environment at the sampling point, with the aim of reducing the loss of vegetation information due to image angle limitations. The calculation formula is as follows:

$$GVI = \frac{Area_g}{Area_t} \times 100\%, \quad (4)$$

where the GVI is the Green View Index, $Area_g$ indicates the green area, and $Area_t$ denotes the total area.

The panoramic view method schematic diagram is shown in Figure 4.

This method has been applied in various research domains. For example, scholars from India proposed a novel indicator to assess vegetation health based on this method [59], while multispectral remote sensing data were used to evaluate the esthetic value of urban green landscapes 11 and study the spatial distribution of urban greening [60,61].

Researchers who prefer the panoramic view method argue that panoramic images offer a comprehensive view of the visual environment of the sampling point, minimizing the loss of vegetation information caused by image angle constraints. However, this method faces issues of distortion, particularly at the top or bottom of the image, with less distortion at the center [62].

Figure 4. Schematic depicting the panoramic view method (data source: Google Street View).

Researchers have proposed several improvements to address these image distortions. Most commonly, panoramic images are captured with a height-to-width ratio of 1:2, covering 360° horizontally and 180° vertically. Certain researchers set the ratio to 1:4, covering 90° vertically and cropping the top and bottom 50% of the image. Others cropped the central part of the panoramic image for measurement, arguing that the cropped section experiences less distortion and is closer to the pedestrian's line of sight [63,64]. Some researchers proposed a transformer-based dual deformable panoramic semantic segmentation network to optimize heavily distorted street view sections [65].

E. Fisheye View Method

The panoramic view method uses equidistant cylindrical projections for analysis, whereas the fisheye view method converts these cylindrical projections into equidistant azimuthal projections to create hemispherical images.

As illustrated below, W_p and H_p represent the width and height of the cylindrical panoramic image, respectively. Consequently, $r_0 = W_p/2\pi$ indicates the radius of the fisheye image, while W_p/π denotes the width and height. The final resolution of the fisheye image center (C_x, C_y) is given as follows:

$$C_x = C_y = \frac{W_c}{2p}, \tag{5}$$

The coordinates (x_f, y_f) on the fisheye image correspond to (x_p, y_p) on the panoramic image and are calculated as follows [66]:

$$x_p = \frac{\theta}{2\pi} W_p, \tag{6}$$

$$y_p = \frac{\theta}{r_0} H_p, \tag{7}$$

$$q = \begin{cases} \frac{p}{2} + tan^{-1}\left(\frac{y_f - C_y}{x_f - C_x}\right), x_f < C_x \\ \frac{3p}{2} + tan^{-1}\left(\frac{y_f - C_y}{x_f - C_x}\right), x_f > C_x \end{cases}, \tag{8}$$

$$r = \sqrt{\left(x_f - C_x\right)^2 + \left(y_f - C_y\right)^2}, \tag{9}$$

The fisheye view method schematic diagram is shown in Figure 5.

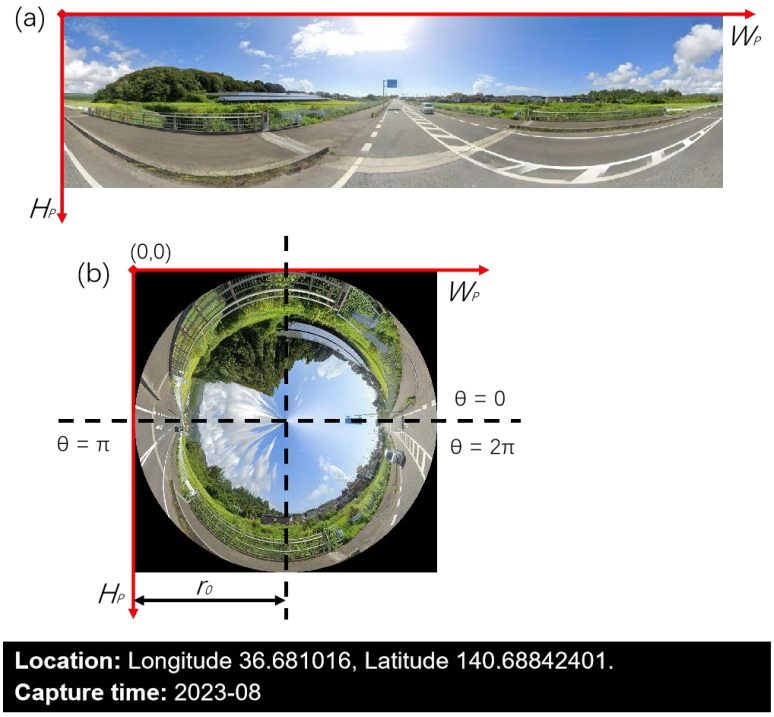

Figure 5. Geometric transformation from Equidistant Cylindrical Projection (**a**) to Equidistant Azimuthal Projection (fisheye image) (**b**) (data source: Google Street View).

Based on this principle, panoramic images can be transformed into fisheye images with a view angled toward the zenith, a process implemented using Python and OpenCV.

The distinctive aspect of this method is that, in addition to the GVI, it can obtain additional metrics, such as sky view factors, enabling climate adaptability studies based on surface temperature and other urban thermal environment indicators [10,67,68]. In addition, it can analyze the impact of urban street environment attributes on pedestrian routes [69].

Although this method comprehensively captures green vegetation information, it suffers from severe image distortion. Given its upward-viewing angle, the area covered by vegetation closer to the ground is larger, whereas the vegetation further from the ground is less represented, making it the least representative of the human visual perspective among the sampling methods.

F. Pedestrian View Method

The pedestrian view method abandons the use of panoramic street view images and instead adopts the tangent direction of the street centerline as the primary direction for capturing street view imagery. This approach aims to closely simulate the horizontal street environment as perceived by pedestrians during their movement. The horizontal field of view is typically set to 120°, mimicking the human eye's visual perspective as closely as possible.

The formula for calculating the GVI using this method is the same as that in the panoramic view method.

A schematic of the pedestrian view method is shown in Figure 6.

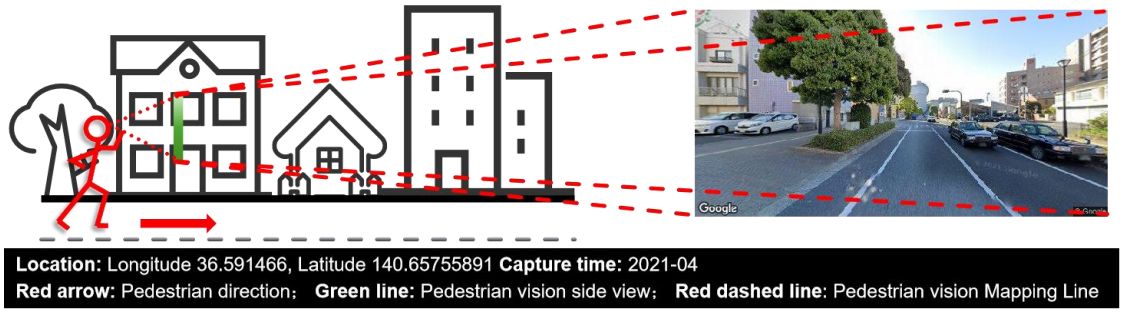

Figure 6. Schematic depicting the pedestrian view method (data source: Google Street View).

The pedestrian view method offers significant advantages in simulating real-world pedestrian experiences in urban environments. By focusing on the tangent direction of the street centerline and limiting the horizontal field of view, this method significantly reduces computational complexity compared to full panoramic views. It is thus a practical and efficient choice for studies with constrained computational resources or those prioritizing the pedestrian perspective.

This method has been applied in human-scale urban studies. For example, Cui et al. used street view imagery to analyze gender differences in perceived safety, while Qiu et al. examined the impact of street environment measures on housing prices, showcasing the method's relevance in diverse urban research areas [17,70]. Additionally, Xu et al. developed a dynamic GVI model based on pedestrian pathways, emphasizing three key factors: field of view, experiential paths, and experiential duration. Notably, the model highlights the role of experiential duration as a primary influence, offering a detailed analysis of how varying durations of exposure to green view environments affect the overall perception of greenery. By capturing the dynamic and continuous nature of human experiences, rather than relying on a single moment to represent the entire process, this approach provides a more realistic and comprehensive indicator for evaluating urban green spaces [71].

Applied research has been scarce because the method is novel. One issue with the method is that the road tangent angle of the pedestrian's direction of travel cannot be obtained in batches, making data collection challenging when extensive amounts of data are required. Addressing the challenges in the batch acquisition of tangent angle data will be essential for applying this method in future studies.

G. Comparative Analysis of Existing Sampling Methods

Existing sampling methods vary significantly in their requirements for street view image acquisition. The pedestrian, panoramic, and fisheye view methods are the most efficient, requiring a number of images equal to that of the sampling points. In contrast, the four-quadrant, six-quadrant, and eighteen-quadrant view methods demand four, six, and eighteen times more images, respectively, which leads to higher research costs, especially when using commercial APIs such as Google's.

Operational complexity also differs among methods. The four-quadrant, six-quadrant, eighteen-quadrant, and panoramic view methods allow for direct GVI calculation after image acquisition, which minimizes processing efforts. However, the fisheye view method involves additional image processing, and the pedestrian view method requires the careful determination of sampling angles, making these methods more labor-intensive.

While the panoramic view method is advantageous due to its low cost and simplicity, a major drawback of this method lies in its significant image distortion. This highlights the need for innovative sampling methods that balance cost, complexity, and accuracy to overcome the limitations of existing approaches.

3.2. Novel Sampling Method: Three-Quadrant View Method

A comprehensive analysis of the five aforementioned street view sampling methods revealed certain inherent limitations. For example, varying degrees of image distortion may lead to misjudgments regarding the greenery within street scenes, while insufficient coverage angles may result in the omission of crucial street scene information. During the large-scale acquisition of street view images, computational accuracy tends to be prioritized at the expense of a high demand for computational resources. Additionally, the excessive pursuit of comprehensive street scene information often diverges from the original intent of simulating human visual perspectives. Consequently, while maintaining computational accuracy, it is essential to propose a novel method that balances perspective coverage with computational requirements. Furthermore, a side-by-side comparison of the GVI results from all sampling methods should be carried out, along with a quantitative analysis of the differences.

This study introduces a novel sampling method based on the conventional human visual perspective of 120°. This method entails joining three 120° street view images to construct a 360° panorama for calculating the GVI. The advantage of this method lies in its closer approximation to the actual field of vision of the human eye, enabling a more comprehensive capture of greenery coverage in street scenes. The calculation formula is as follows:

$$GVI = \frac{Area_{g\_i}}{Area_{t\_i}} \times 100\% = \frac{\sum GVI_i}{i}(i = 3), \tag{10}$$

The fundamental premise of this method is to simplify the computational process by reducing the frequency of perspective segmentation while simultaneously ensuring the accuracy of the resulting calculations. The three-quadrant view method schematic diagram is shown in Figure 7 below.

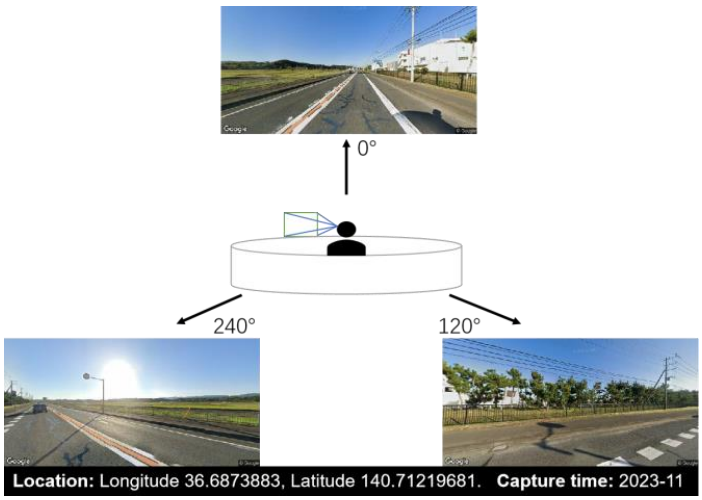

Figure 7. Schematic depicting the three-quadrant view method (data source: Google Street View).

Compared to traditional methods for calculating GVI, the proposed approach offers several advantages:

- Reduction in computational complexity: while conventional methods require the processing of numerous images, this method requires only three images, thereby significantly decreasing the computational burden.
- Alignment with the human visual perspective: the 120° field of view closely mirrors the natural sightline of the human eye, which makes the results more relevant and applicable to real-world scenarios [72].

4. Methodology

4.1. Research Framework

In this study, a comprehensive research framework was designed to systematically evaluate the impacts of different sampling methods on urban street GVI calculations. During the street view data collection phase, we selected 190 representative sampling points covering different road types within the city to ensure the diversity and representativeness of the samples. Subsequently, we employed seven sampling methods to collect street view data for each sampling point, allowing us to compare the effects of various sampling methods on the GVI results.

In the GVI extraction phase, we utilized a street view GVI recognition tool to analyze the collected images. To ensure consistency, the same recognition tool was used across all sampling methods to eliminate the bias introduced by differences between tools.

In the data analysis phase, we first performed a descriptive statistical analysis of the GVI results obtained from each sampling method to assess basic statistical characteristics, such as the mean and standard deviation. Next, we conducted a difference analysis (e.g., one-way analysis of variance (ANOVA) and paired t-tests) to determine whether the differences in GVI between the sampling methods were statistically significant. Additionally, we performed a correlation analysis (Pearson correlation coefficient analysis) to evaluate the relationships between the results from different sampling methods and to explore their consistencies and discrepancies. The research framework is shown in Figure 8.

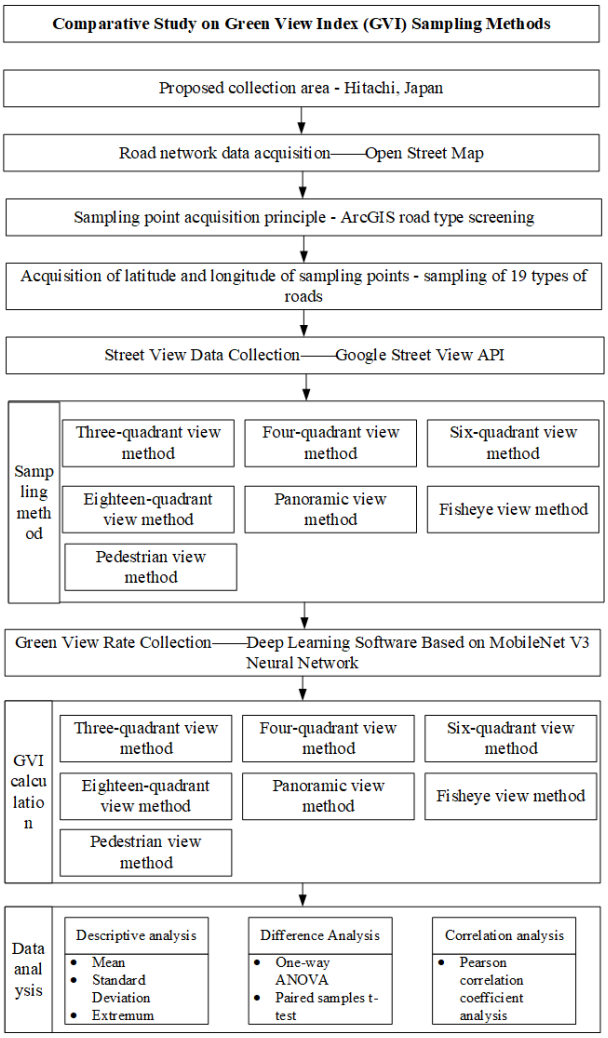

Figure 8. Research framework.

4.2. Data Acquisition

To mitigate the data bias caused by the characteristics of different road types, we first selected Hitachi City, Japan, as the area for data collection. Hitachi City, located in the northern part of Ibaraki Prefecture in northeastern Japan, lies along the Pacific Ocean to the east. The city spans a total area of 225.73 km^2 and is characterized by an elongated urban layout stretching from north to south. Hitachi has a well-developed road network with a total length of 1697.5 km and a road density of 3.5 km/km^2. The city experiences a temperate maritime climate with distinct seasonal variations, which contributes to the rich and diverse green vegetation within the urban landscape [73].

The city's road network information was obtained using the OpenStreetMap webpage [74]. Due to the high sensitivity of street view target features, a limited number of sampling points may reduce the reliability of the metrics constructed from the data, making the experimental results less applicable to broader populations or contexts and affecting the external validity of the study [75]. Using the ArcGIS 10.4 software, we identified various road types and selected ten sampling points for each of these types, which resulted in 190 data points with different latitudes and longitudes. We then employed the GSV Application Programming Interface platform to retrieve static street images corresponding to these coordinates.

The road types and sampling points are listed in Table 1.

Table 1. Road types and sampling points.

Class	Number of Sample Points	Class	Number of Sample Points
motorway	10	residential	10
Motorway link	10	service	10
trunk	10	track	10
Trunk link	10	cycleway	10
primary	10	pedestrian	10
secondary	10	path	10
Secondary link	10	steps	10
tertiary	10	unknown	10
Tertiary link	10	footway	10
unclassified	10	SUM	190

We thus used 190 sets of street view data, with the earliest capture date being 28 February 2018, and the latest being 30 June 2024. To ensure optimal data collection for GVI measurement, we acquired street view data between March and August each year. This period coincided with the growing season in the Northern Hemisphere and allowed for the collection of abundant green space data. Although some data were collected during the winter months, evergreen vegetation could still be captured. Notably, we focused on comparing different sampling methods but did not analyze the overall urban greening level.

4.3. Sampling Methods

Based on previous research, seven sampling methods were selected, as listed in Table 2. The vertical coverage angle was set to 60°, slightly exceeding the comfortable range of eye rotation (55°) and thereby aligning more closely with the human visual perspective. Notably, the vertical coverage angle for the panoramic view method was 90°, while the fisheye perspective method transformed panoramic images into fisheye images viewed from a zenith perspective. This process was implemented using Python3.7 and OpenCV.

Table 2. Summary of GVI sampling methods.

NO.	Sampling Method	Horizontal Coverage Angle	Vertical Coverage Angle	Horizontal Angle	Number of Captured Images
1	Three- quadrant view method	120	60	0	3
2	Four-quadrant view method	90	60	0	4
3	Six-quadrant view method	60	60	0	6
		60	60	0	6
4	Eighteen-quadrant view method	60	60	45	6
		60	60	−45	6
5	Panoramic view method	360	90	0	1
6	Fisheye view method				1
7	Pedestrian view method	120	60	0	1

4.4. GVI Extraction

Traditional methods for extracting the GVI involve pixel or grid-based calculations of images using software such as Photoshop or GNU Image Manipulation Program (GIMP). These approaches require manual grid delineation and selection, which is both time-consuming and error-prone. Currently, more advanced methods use deep learning algorithms for GVI extraction, including PSPNet 37, SegNet [76], FCN8 [77], Backpropagation Neural Networks [78], and Deepak [79]. To ensure experimental consistency, the same deep learning tool was used for GVI extraction.

This study employed a deep learning software based on the MobileNet V3-Large neural network, developed by the National Institute for Land and Infrastructure Management, Japan, in 2022 [80]. The neural network structure employed in MobileNet V3-Large is a lightweight neural network algorithm designed for efficient computation [81]. By strategically eliminating redundant components, it significantly reduces the computational load. While this approach entails a slight compromise in terms of accuracy, it enables the practical processing of images on mobile devices, making it a highly suitable choice for resource-constrained environments.

The training dataset for this software comprised green-view survey photographs provided by local Japanese governments that capture urban landscapes and vegetation in areas such as Shinjuku, Koto, and Musashino in Tokyo. These photographs were taken in various seasons and weather conditions and amounted to 150 images. The original images were augmented using image enhancement techniques to enhance the model's generalizability and accuracy. This resulted in an expanded dataset of 5000 images, offering a rich pool of training data.

4.5. GVI Calculation

After obtaining the GVI for each image, we calculated the GVI for each of the seven sampling methods according to the aforementioned equations. The results are summarized in Table 3.

Table 3. Comparison of GVI Results Across Seven Sampling Methods.

	Three-Quadrant View Method	Four-Quadrant View Method	Six-Quadrant View Method	Eighteen-Quadrant View Method	Panoramic View Method	Fisheye View Method	Pedestrian View Method
motorway	31.84	34.81	35.60	18.80	25.99	42.68	27.94
motorway link	29.69	32.58	33.31	15.63	24.66	42.84	28.64
trunk	22.59	22.96	23.98	21.59	18.56	32.67	22.17
trunk link	6.16	5.48	5.20	9.28	4.33	12.80	10.10

Table 3. *Cont.*

	Three-Quadrant View Method	Four-Quadrant View Method	Six-Quadrant View Method	Eighteen-Quadrant View Method	Panoramic View Method	Fisheye View Method	Pedestrian View Method
primary	42.70	45.55	45.48	24.73	35.77	52.20	41.14
secondary	28.48	28.59	27.98	24.28	23.62	31.88	24.88
secondary link	33.05	32.36	31.73	31.93	31.12	26.17	30.01
tertiary	25.96	27.81	27.49	20.61	21.41	33.41	27.94
tertiary link	18.20	19.47	19.55	13.05	14.67	27.43	20.25
unclassified	36.07	37.92	39.55	24.80	30.60	46.23	34.13
residential	25.22	26.00	25.52	18.34	19.25	30.52	25.35
service	29.17	31.25	31.22	20.26	25.85	37.55	29.83
track	39.10	38.69	37.73	25.41	37.60	44.16	37.76
cycleway	18.65	18.24	16.89	11.30	18.28	29.82	28.09
pedestrian	19.81	19.68	19.64	19.96	12.40	15.54	21.05
path	57.04	59.29	59.99	38.06	50.98	58.06	52.49
steps	36.54	37.11	37.50	28.32	31.47	37.91	27.49
unknown	30.04	32.59	31.63	20.65	25.64	37.71	25.20
footway	33.87	36.64	37.49	22.80	29.08	42.66	36.75

5. Results

5.1. Visual Analysis

We conducted a comprehensive visual analysis of the GVI for 19 distinct road types using bar charts. This approach enabled a clear comparison of the differences among the seven GVI calculation methods. Additionally, we calculated the standard deviation for each road type across the different methods, presenting the results in a separate bar chart to highlight the variability. These findings are detailed in the subsequent sections, with the results illustrated in Figure 9.

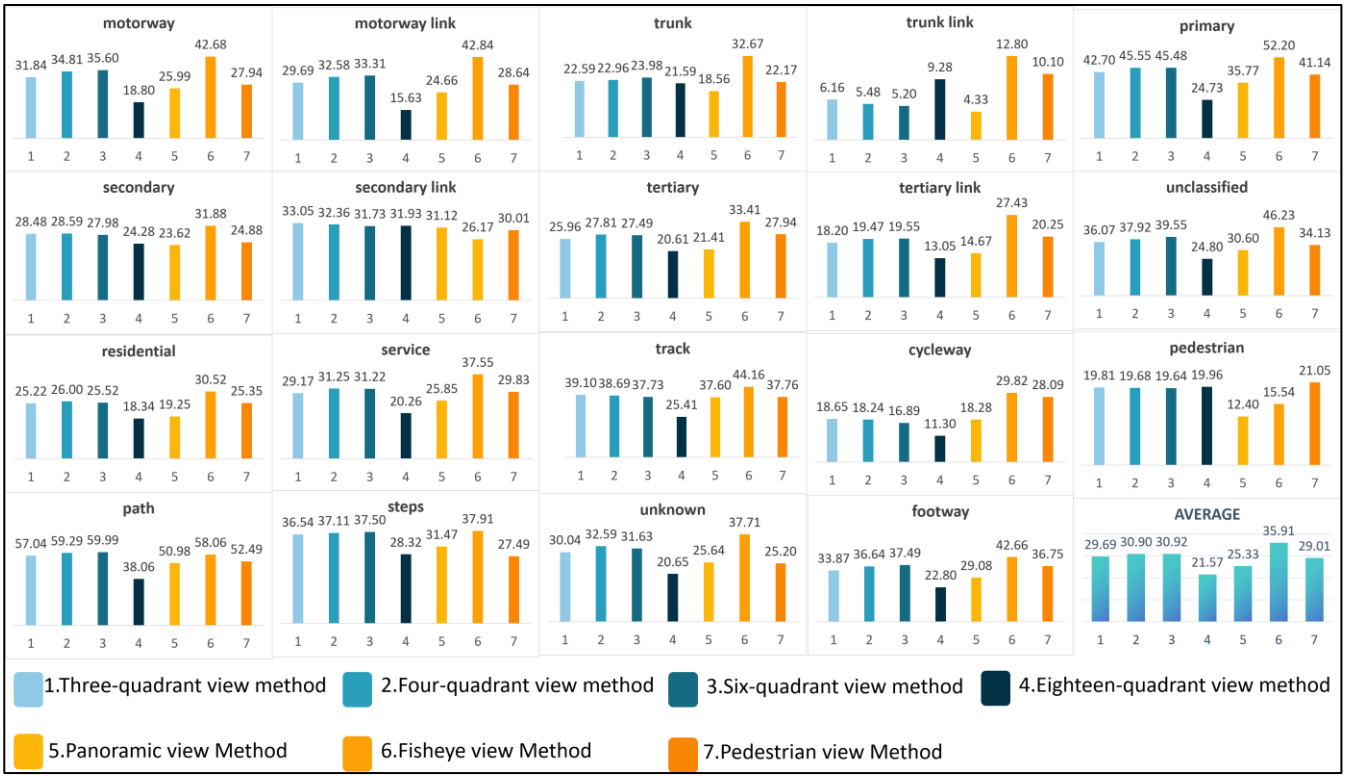

Figure 9. Line chart of different sampling methods.

Our analysis of GVI values across 19 road types revealed significant variability among the seven measurement methods. Quadrant-based approaches, particularly the six-quadrant (30.92) and four-quadrant (30.90) methods, demonstrated the highest mean GVI values, which indicate balance in the detail and overall greenery representation. The three-quadrant method (29.69) also performed consistently, making it a suitable choice when fewer divisions are required. In contrast, the eighteen-quadrant method (21.57) consistently underperformed, especially for motorways, due to the excessive spatial segmentation, which fragments the view and reduces the overall GVI.

Among the remaining methods, the fisheye view method achieved the highest overall mean GVI (35.91), comprehensively capturing greenery, particularly in open or extensive areas. However, the increased GVI value in this method may be affected by image distortion and thus may incorrectly represent the actual greening status. The pedestrian perspective method (29.01) and panoramic view method (25.33) provided moderate results. While the pedestrian perspective method closely approximated the real-world perception of greenery, both methods were less effective at capturing fine details compared to quadrant-based approaches.

Overall, the choice of GVI measurement method significantly impacts the results, with each approach having distinct advantages and limitations. Quadrant-based methods excel in balancing segmentation and detail, making them reliable for diverse road types. In contrast, the fisheye view method is suited for broader greenery assessments, despite potential distortion issues. The findings emphasize the need to select methods that are tailored to specific road types and assessment objectives to ensure accurate and meaningful GVI evaluations.

5.2. Descriptive Statistics

Descriptive statistical analyses were performed on the GVI calculated using the seven sampling methods to elucidate the basic characteristics of each method. The statistics included the mean, standard deviation, and minimum and maximum values for each method. The results are listed in Table 4.

Table 4. Descriptive statistics.

	Value	Minimum	Maximum	Mean	Standard Deviation
Three-quadrant view method	19	6.164	57.037	29.69	10.85
Four-quadrant view method	19	5.484	59.293	30.90	11.52
Six-quadrant view method	19	5.199	59.989	30.92	11.80
Eighteen-quadrant view method	19	9.282	38.059	21.57	6.90
Panoramic view method	19	4.327	50.984	25.33	10.29
Fisheye view method	19	12.800	58.060	35.91	11.29
Pedestrian view method	19	10.096	52.486	29.01	9.00

From Table 4, it can be observed that the fisheye view method demonstrated the highest average GVI (35.91), whereas the eighteen-quadrant view method showed the lowest average GVI (21.57). The four-quadrant view method exhibited the widest distribution of the GVI, with a standard deviation of 11.52. Overall, the mean and standard deviation of the GVI varied significantly across the seven methods, indicating considerable differences in performance among the sampling methods.

When studying the same road type, there are still differences between the results of the different methods. We used standard deviation for statistical analysis and obtained the conclusions shown in Figure 10.

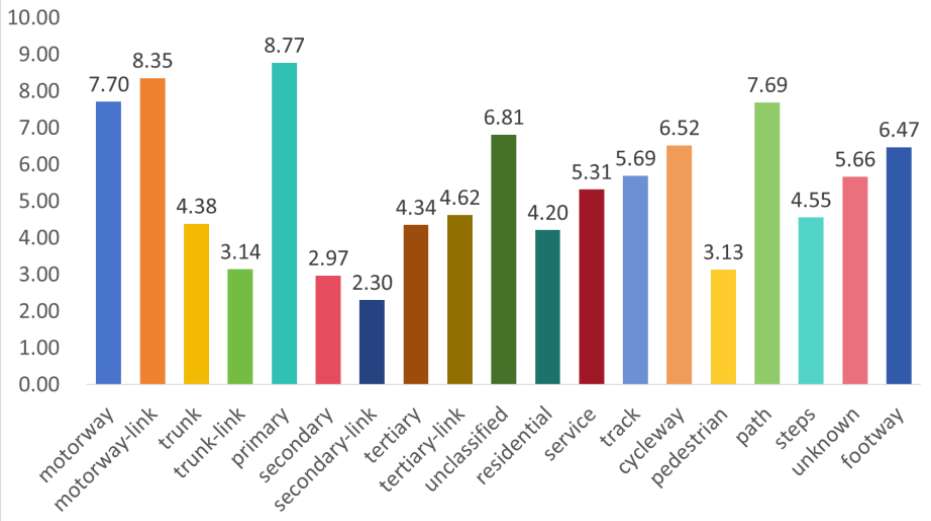

Figure 10. Histogram of standard deviations across sampling methods for different road types.

Our analysis indicates that the sampling methods exhibited varying degrees of variability for different road types. The lowest standard deviation was observed for secondary links (2.3), indicating minimal variation across sampling methods. In contrast, eight road types had standard deviations exceeding 6, with primary roads showing the highest value (8.77). This suggests that, for these road types, the choice of sampling method can significantly influence the GVI.

5.3. Difference Analysis

To assess whether there were significant differences in GVI among the sampling methods, we conducted a one-way ANOVA. The results indicated that the GVI differences among the sampling methods were statistically significant ($F(6, 126) = 3.661$, $p < 0.05$). The results are listed in Table 5.

Table 5. One-way ANOVA results.

	Sum of Squares	Degrees of Freedom	Mean Square	F-Statistic	*p*-Value
Between groups	2358.592	6	393.099	3.661	0.002
Within groups	13,528.047	126	107.365		

To further identify methods with significant differences, a Tukey post hoc test was conducted. The results revealed a significant difference in GVI between the fisheye view method and both the eighteen-quadrant method and the panoramic view method ($p < 0.05$). While other method comparisons also exhibited differences, these were not statistically significant. The detailed results are presented in Table 6.

Figure 11 presents a box plot of the GVI values across different sampling methods. The box plot illustrates the median, interquartile range, and minimum and maximum values for each method. The three-quadrant view method, four-quadrant view method, six-quadrant view method, fisheye view method and pedestrian view method had higher medians, whereas the eighteen-quadrant view method had a lower median. The fisheye view method showed a wider distribution, indicating greater variability in the data.

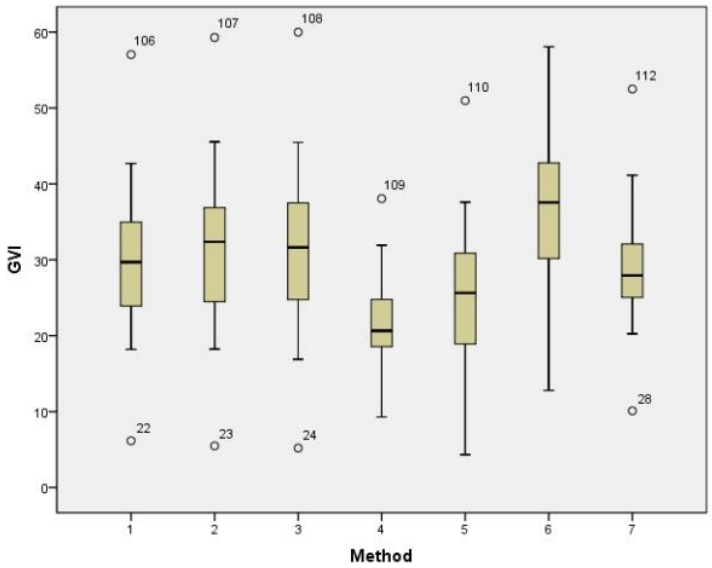

Figure 11. Box plot showing the distribution of the GVI values across different sampling methods.

Table 6. Tukey's post hoc test results.

(I) Method	(J) Method	Mean Difference (I-J)	Std. Error	Sig.	95% Confidence Interval	
					Lower Bound	Upper Bound
1	2	−1.202555	3.361789	1	−11.27628	8.87117
	3	−1.225575	3.361789	1	−11.29930	8.84815
	4	8.124892	3.361789	0.200	−1.94883	18.19861
	5	4.362664	3.361789	0.852	−5.71106	14.43638
	6	−6.213324	3.361789	0.518	−16.28704	3.86040
	7	0.683932	3.361789	1	−9.38979	10.75765
2	1	1.202555	3.361789	1	−8.87117	11.27628
	3	−0.023020	3.361789	1	−10.09674	10.05070
	4	9.327447	3.361789	0.089	−0.74627	19.40117
	5	5.565219	3.361789	0.647	−4.50850	15.63894
	6	−5.010769	3.361789	0.750	−15.08449	5.06295
	7	1.886487	3.361789	0.998	−8.18723	11.96021
3	1	1.225575	3.361789	1	−8.84815	11.29930
	2	0.023020	3.361789	1	−10.0507	10.09674
	4	9.350467	3.361789	0.088	−0.72325	19.42419
	5	5.588238	3.361789	0.642	−4.48548	15.66196
	6	−4.987749	3.361789	0.754	−15.06147	5.08597
	7	1.909507	3.361789	0.998	−8.16421	11.98323
4	1	−8.124892	3.361789	0.200	−18.19861	1.94883
	2	−9.327447	3.361789	0.089	−19.40117	0.74627
	3	−9.350467	3.361789	0.088	−19.42419	0.72325
	5	−3.762229	3.361789	0.921	−13.83595	6.31149
	6	−14.338216 *	3.361789	0.001	−24.41194	−4.26450
	7	−7.440960	3.361789	0.296	−17.51468	2.63276
5	1	−4.362664	3.361789	0.852	−14.43638	5.71106
	2	−5.565219	3.361789	0.647	−15.63894	4.50850
	3	−5.588238	3.361789	0.642	−15.66196	4.48548
	4	3.762229	3.361789	0.921	−6.31149	13.83595
	6	−10.575988 *	3.361789	0.033	−20.64971	−0.50227
	7	−3.678731	3.361789	0.929	−13.75245	6.39499

Table 6. *Cont.*

(I) Method	(J) Method	Mean Difference (I-J)	Std. Error	Sig.	95% Confidence Interval	
					Lower Bound	Upper Bound
6	1	6.213324	3.361789	0.518	−3.86040	16.28704
	2	5.010769	3.361789	0.750	−5.06295	15.08449
	3	4.987749	3.361789	0.754	−5.08597	15.06147
	4	14.338216 *	3.361789	0.001	4.26450	24.41194
	5	10.575988 *	3.361789	0.033	0.50227	20.64971
	7	6.8972560	3.361789	0.388	−3.17646	16.97098
7	1	−0.683932	3.361789	1	−10.75765	9.38979
	2	−1.886487	3.361789	0.998	−11.96021	8.18723
	3	−1.909507	3.361789	0.998	−11.98323	8.16421
	4	7.440960	3.361789	0.296	−2.63276	17.51468
	5	3.678731	3.361789	0.929	−6.39499	13.75245
	6	−6.897256	3.361789	0.388	−16.97098	3.17646

* The mean difference is significant at the 0.05 level.

5.4. Correlation Analysis

To evaluate the correlation between the GVI values calculated using different sampling methods, we computed the Pearson correlation coefficients. The correlation matrix distinctly demonstrated the relationships among the methods, as shown in Table 7.

Table 7. Pearson correlation coefficient matrix.

	Three-Quadrant View Method	Four-Quadrant View Method	Six-Quadrant View Method	Eighteen-Quadrant View Method	Panoramic View Method	Fisheye View Method	Pedestrian View Method
Three-quadrant view method	1	0.995 **	0.990 **	0.861 **	0.985 **	0.887 **	0.936 **
Four-quadrant view method	0.995 **	1	0.998 **	0.823 **	0.972 **	0.915 **	0.933 **
Six-quadrant view method	0.990 **	0.998 **	1	0.819 **	0.963 **	0.919 **	0.925 **
Eighteen-quadrant view method	0.861 **	0.823 **	0.819 **	1	0.852 **	0.570 *	0.737 **
Panoramic view method	0.985 **	0.972 **	0.963 **	0.852 **	1	0.875 **	0.941 **
Fisheye view method	0.887 **	0.915 **	0.919 **	0.570 *	0.875 **	1	0.879 **
Pedestrian view method	0.936 **	0.933 **	0.925 **	0.737 **	0.941 **	0.879 **	1

**. The correlation is significant at the 0.01 level (two-tailed). *. The correlation is significant at the 0.05 level (two-tailed).

Pearson correlation analysis indicated strong positive relationships among the quadrant-based methods. Specifically, the three-quadrant, four-quadrant, and six-quadrant methods exhibited high correlations from 0.990 to 0.998, indicating that these methods yielded similar GVI results. The results of the four-quadrant and six-quadrant methods were almost identical, with a correlation of 0.998, suggesting that these methods can be used interchangeably in capturing greenery data. The results of the three-quadrant method also strongly correlated with those of the other quadrant-based methods, albeit with slightly lower correlation coefficients.

The results of the eighteen-quadrant method were less tightly correlated with those of the other quadrant-based methods, with values ranging from 0.819 to 0.861. Excessive segmentation in the eighteen-quadrant method likely leads to a divergence in GVI measurements and a lower consistency compared to methods that use fewer divisions. The results obtained using this method had the lowest correlation with those of the

fisheye view method (0.570), highlighting a potential difference in the type of data the methods capture.

The results of the panoramic view method showed moderate to strong correlations with those of the quadrant-based methods, ranging from 0.852 to 0.985. The results of the eighteen-quadrant method had the lowest correlation with those of the panoramic method (0.852), suggesting that over-segmentation in the eighteen-quadrant method creates a weaker relationship with broader view methods. However, the panoramic view method, similarly to the quadrant-based approaches, consistently provided reliable GVI assessments in wider spatial contexts.

The results of the fisheye view method were moderately to strongly correlated with those of the other methods, particularly with those of the six-quadrant method (0.919), while the results were less tightly correlated with those of the eighteen-quadrant method (0.570). This lower correlation could be because the fisheye view method captures a broader, panoramic perspective, which differs significantly from the more fragmented views provided by the eighteen-quadrant method. Nevertheless, the fisheye view method is still a valuable method for capturing expansive greenery areas, although it does not align perfectly with more segmented approaches.

The results of the pedestrian view method were also strongly correlated with those of the other methods, particularly with those of the quadrant-based methods (0.933 to 0.941). This consistency suggests that the pedestrian method offers a reliable measure of greenery that aligns closely with traditional segmentation methods, making it a suitable choice for real-world, on-the-ground assessments. However, the results of the fisheye and panoramic view methods were slightly less tightly correlated with those of the eighteen-quadrant method, which again indicates the importance of selecting an appropriate method based on the spatial context and assessment needs.

6. Construction and Evaluation of the "Green View Circle" Model Based on Optimized Sampling

6.1. Problem Statement

This study compared the performance of various sampling methods in the calculation of the GVI, including the quartered view method, sextant view method, eighteen-segment view method, panoramic view method, and fisheye view method. The results indicated that different sampling methods significantly influenced the GVI outcomes. Traditional segmented sampling approaches typically employ a default starting sampling angle (commonly oriented to true north) as a benchmark for street view segment sampling. However, whether altering the initial sampling angle has a notable impact on the final GVI remains an open question. To investigate this, the following validation experiments were conducted:

- Test Location: Longitude 36.578949; latitude 140.61494869.
- Experimental Groups:

  Group A: Vertical angle of 60°; horizontal angle of 120°.
  Group B: Vertical angle of 60°; horizontal angle of 90°.
  Group C: Vertical angle of 60°; horizontal angle of 60°.
- Sampling Method: Data were collected from 360 distinct initial sampling angles ranging from 0° (true north) to 360°, resulting in 360 street view images and corresponding GVI calculations.
- Calculation Method: The GVI was computed for each group using their respective viewing methods. Group A produced GVI values for 120 different initial angles, Group B for 90 angles, and Group C for 60 angles.

Figure 12 shows a schematic of the experimental design.

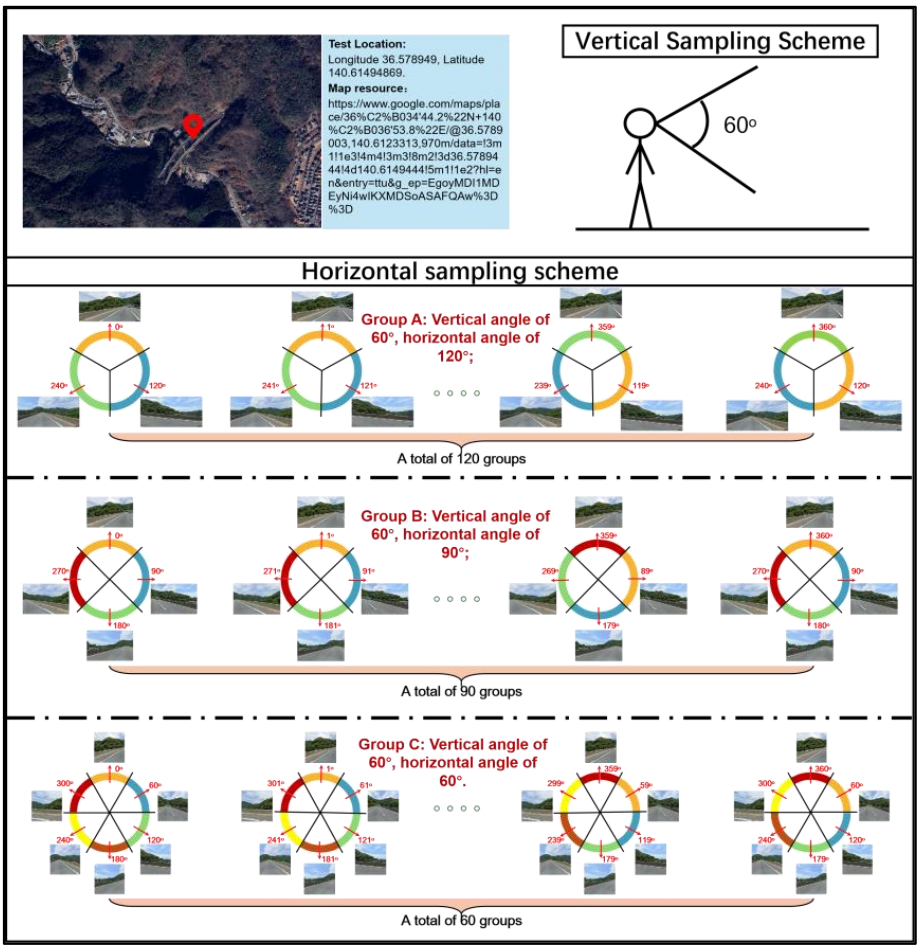

Figure 12. Schematic of the verification experiment of the effect of the initial sampling angle on GVI results.

After analyzing the GVI data obtained from three groups, we calculated the GVI values for different initial sampling angles of 120°, 90°, and 60°, starting from zero degrees and proceeding clockwise. As shown in Figure 13, the values differed significantly.

The results demonstrated significant variations in GVI values across different initial angles. The characteristic GVI values for the three groups were as shown in Table 8.

Table 8. Validation of experimental statistical results.

Group	Count	Mean	Maximum	Minimum	Range	Standard Deviation
Group A	120	28.484	31.267	24.821	6.446	2.095
Group B	90	25.728	27.842	23.470	4.372	1.401
Group C	60	23.327	23.661	22.779	0.882	0.263

Significant disparities in the calculated GVI arose when employing different street view sampling methods at the same sampling point. Additionally, variations in the initial angles of the sampling points resulted in changes in the GVI values. This discrepancy was particularly pronounced when the number of sampled images was limited, making the errors induced by the initial angle especially salient.

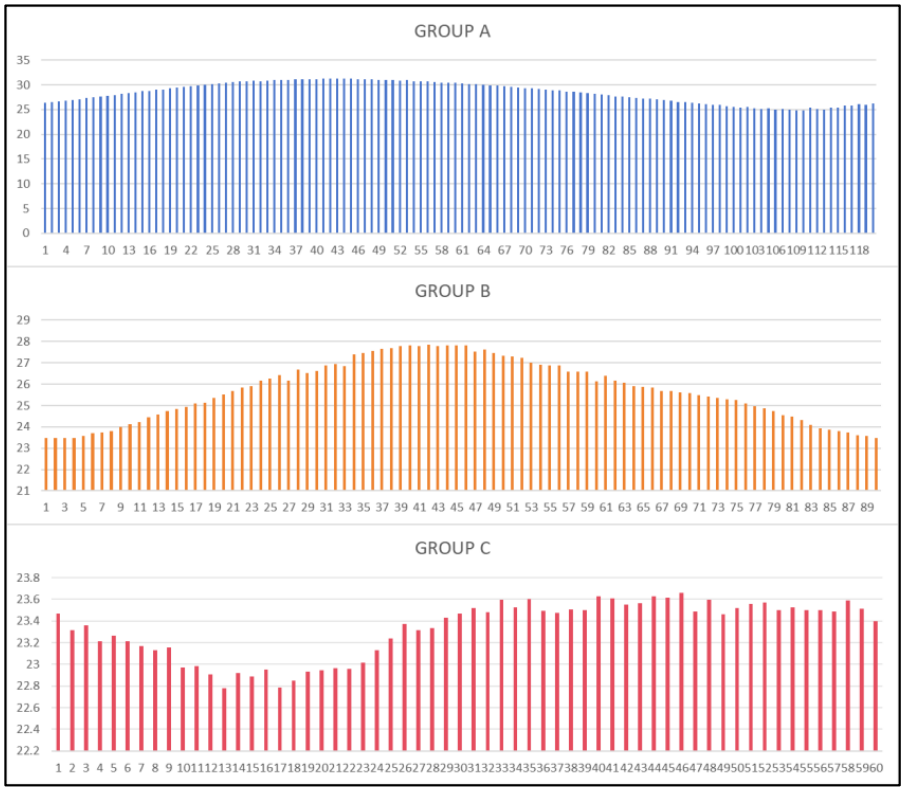

Figure 13. Three sets of GVI change histograms with different initial sampling angles.

Upon analyzing the eigenvalues, we observed significant differences in the mean GVI across groups. Notably, the mean GVI tended to increase with wider coverage angles. This is partly because a broader viewing angle captures a larger spatial area, thus including finer or peripheral greenery elements that may otherwise be overlooked. Meanwhile, a wider angle can also reduce the resolution of details, particularly at the boundaries between green and non-green areas. In addition, notable variations were observed in the GVI range and standard deviations across groups. Groups with a larger horizontal angle exhibited a greater range and standard deviation, primarily due to the edge distortion inherent in the transformation of three-dimensional images to a two-dimensional format. As the horizontal scope widens, the distortion intensifies, meaning that Group A, with more edge distortion, showed a greater GVI measurement error than Group C, where the distortion effects were less pronounced.

Considering this analysis, it is evident that, irrespective of the sampling method employed, fixing the initial sampling angle invariably leads to uncontrollable errors. The numerous prior studies utilizing the GVI for urban greening assessments frequently overlooked these inaccuracies. Thus, it can be argued that GVI methodologies relying on a fixed initial sampling angle lack the necessary rigor.

In response to these challenges, this study proposes a novel concept for greening assessment, aimed at mitigating errors arising from sampling angles and quantities.

6.2. Model Overview

Building on existing GVI calculation methods, this study introduces a novel approach termed the GVC. This method aims to enhance both computational accuracy and spatial coverage. By employing segmented sampling from a 360-degree perspective for each observation point and calculating the GVI at each angle, this approach effectively reflects the distribution of greenery within the observed environment.

The essence of the GVC method lies in its comprehensive coverage of the observation points from a full 360-degree perspective. The entire field of view is divided into smaller angular segments (e.g., 1-degree, 5-degree, and 10-degree intervals), facilitating the acquisition of more precise GVI results. Ultimately, the greening level is represented by the area of a polygon, thereby refining the observation area and providing an accurate greenery index.

6.3. Model Construction and Formula Derivation

At the observation point, we uniformly partitioned the 360° field of view into N angular segments and utilized different segments as sampling directions for street view data collection. Given that the typical horizontal visual angle of the human eye is 120°, with a comfortable vertical rotation range of approximately 55°, we selected vertical and horizontal angles of 60° and 120°, respectively, for each sampling session.

Let the GVI for each angular segment be denoted as GVI_i. We defined a circle with a radius of one, centered at the observation point, with true north designated as 0° and angles measured in a clockwise direction. For each sampling angle, we used the corresponding GVI data as the side lengths to construct a polygon. The area of the polygon was computed based on the connections between the green view indices of adjacent angles using the following area calculation formula:

$$A = \frac{1}{2} \times \sum_{i=1}^{N} GVI_i \times GVI_{i+1} \times \sin \frac{360^\circ}{N} (N \geq 3), \tag{11}$$

where GVI_i and GVI_{i+1} represent the adjacent values of the GVI, with $i = N$, implying that $i + 1 = 1$.

When all the GVI values equal 100%, the area of the polygon is defined as follows:

$$A_{\max} = \frac{N}{2} \times \sin \frac{360^\circ}{N} (N \geq 3), \tag{12}$$

As N increases, indicating the finer sampling of angular directions, the resulting polygon approaches a perfect circle, with its area converging toward π. Consequently, by normalizing the area dimensionally, the formula for the GVC can be expressed as follows:

$$GVC = \frac{A}{A_{\max}} = \frac{1}{N} \times \sum_{i=1}^{N} GVI_i \times GVI_{i+1} (N \geq 3), \tag{13}$$

The area calculation in this method was based on the polygon area formula, which was obtained by subdividing the 360-degree perspective of the observation point into smaller angular segments. An overall green-view circular model was constructed by calculating the local GVI at each angle.

Using the aforementioned experimental points as examples, the horizontal space was divided into 360 segments. Using this calculation, the value of the GVC was determined to be 0.08663, as shown in Figure 14.

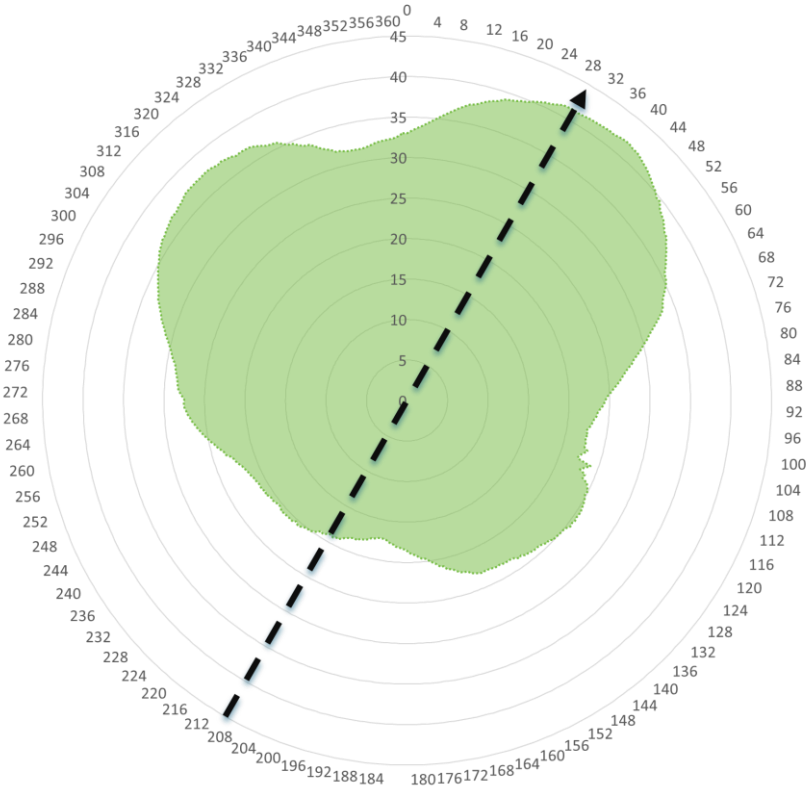

Figure 14. Schematic diagram depicting the Green View Circle.

6.4. Evaluation of the "Green View Circle" Model

The green area in Figure 14 represents the GVC area of the sampling point, and the black arrow indicates the tangent direction of the road centerline at the sampling point. Based on this figure, the following characteristics of the GVC at the respective sampling point can be observed:

1. The GVI values vary across different directions. Regardless of the initial sampling angle selected for traditional GVI calculation, the GVI value cannot represent the actual greening condition at the site, nor can it provide spatial information on the greening around the sampling point based on the calculated values.
2. Due to the overlapping viewing angles between adjacent points, the GVC presents an irregular shape, similar to a curve, with no points suddenly increasing or decreasing in size.
3. As the road progresses from southwest to northeast, the GVC edge is closer to the outer side, indicating denser vegetation in the northeastern direction. Conversely, vegetation is sparse in the southwestern direction of the sampling point.
4. Along the road's normal direction, the GVC curve is closer to the outer side of the circle, indicating abundant vegetation on both sides of the road. However, as the curve deviates slightly from the normal direction, it sharply contracts inward, indicating that the dense vegetation in the normal direction is farther from the sampling point and not related to the vegetation along the road.

Based on this analysis and the GVC of the point, the overall greening condition of the point can be objectively analyzed. This cannot be achieved using the GVI, as the GVI lacks spatial attributes. Therefore, the GVC is the optimal solution for spatial analysis of the GVI.

6.5. Advantages and Disadvantages of the Model

The proposed GVC method demonstrates enhanced accuracy and applicability compared to traditional GVI calculation techniques, especially in urban environments with complex vegetation distributions. By using a detailed sampling strategy that covers a full 360-degree perspective from the observation points, this method effectively captures variations in vegetation across different angles, reducing the biases typically associated with a single viewpoint.

The advantages of the GVC method include the following:

1. High Accuracy: Subdividing the viewing angles at observation points allows for the individual sampling of each angle, significantly enhancing the precision of GVI calculations, particularly in heterogeneous environments.
2. Broad Applicability: This method is particularly well-suited for urban areas with complex vegetation patterns, as it accurately represents greenery from various perspectives and provides a more comprehensive dataset for urban greening assessments.
3. Result Visualization: Visualization techniques, such as radar charts, help present the GVI distribution and variation across different angles, improving the interpretability and dissemination of the research findings.

However, there are several challenges in the practical application of the GVC method:

1. Lack of established evaluation standards: Since the GVC concept introduced in this study is novel and has not been explored in previous research, its practical application may be challenging due to the absence of established evaluation standards.
2. Increased Computational Complexity: Unlike traditional methods, the GVC method involves the calculation of polygon areas, leading to a more complex computation process that may not be suitable for real-time analysis.

Overall, the GVC method offers significant advantages in terms of accuracy and applicability, but its increased data processing and computational complexity pose challenges, particularly for large-scale urban GVI studies and real-time applications.

7. Discussion

7.1. Comparison and Analysis of the Application of Different Sampling Methods

This study compares several sampling methods for calculating the GVI, including the four-, six-, and eighteen-quadrant, panoramic, fisheye, and pedestrian view methods, and the novel three-quadrant view method. This novel method divides the 360° field of view into three equal, 120°-spanning parts, offering a balance between coverage and computational complexity. Our results show that the choice of method significantly influences the GVI calculations [16].

The four- and six-quadrant view methods have been widely used due to their simplicity and low computational cost, making them efficient for large sample sizes. However, the four-quadrant method may miss green information due to its limited coverage, while the six-quadrant method has increased coverage but increased data processing complexity.

The eighteen-quadrant method further expands coverage by incorporating upward and downward views but may underestimate the GVI due to non-vegetative information, such as related to sky and road surfaces. This method also significantly increases the data volume.

The panoramic and fisheye methods provide a broader perspective but are associated with image distortion and an increased processing complexity. Panoramic views require cropping to reduce distortion, and fisheye views capture more information about the sky, which does not accurately reflect human visual perception.

By focusing on the tangent direction of the street centerline and using a horizontal field of view of 120°, the pedestrian view method reduces computational complexity compared to panoramic methods. This approach is ideal for simulating the pedestrian's experience and more suitable for studies with limited computational resources.

The three-segment view method divides the 360° field of view into three equal 120° segments, aiming to provide comprehensive coverage while minimizing image distortion and processing complexity. This method offers a balance between providing a detailed perspective of panoramic views and the lower computational demands of quadrant-based methods. It is especially useful for large-scale urban greening assessments, where both precision and computational efficiency are essential.

Each method has practical advantages depending on the research objectives. For large-scale urban greening assessments, the four- and six-quadrant view methods seem preferable due to their efficiency and low cost. The eighteen-quadrant and panoramic view methods are better suited for a more precise estimation of green coverage, while the fisheye method is valuable for climate adaptability studies. The pedestrian view method offers a good balance between computational efficiency and a realistic pedestrian experience, making it particularly suitable for studies focusing on human-scale urban environments. The proposed new method, based on dividing the field of view into three 120° segments, balances precision and cost, and thus offers a viable solution for large-scale urban greening assessments.

7.2. Current Challenges in GVI Research

Multiple methods exist for collecting urban greening data, with those based on the NDVI and the GVI being the most common. For example, researchers can assess the quantity and quality of urban green spaces by analyzing changes in NDVI values, which reflect the health and ecological function of green spaces [82]. Likewise, the GVI simulates the human eye's perspective for analyses of urban greening. The NDVI, however, lacks precise spatial attributes and is often treated as a two-dimensional plane when used for greening analyses. In contrast, the GVI, as a three-dimensional index, does not have this limitation. Numerous studies have also revealed the inherent relationships between the two indices [83].

However, in large-scale studies using the GVI, data are often presented in a two-dimensional plane, with flat distribution maps of GVI points [3,84,85]. This neglects the three-dimensional characteristics of the GVI and the purpose it was originally designed for. We believe that the GVC theory proposed in this study provides the optimal solution to overcome these and other challenges faced in GVI research.

7.3. GVC Model Application Scenarios

The GVC method offers substantial practical value for government agencies, particularly in the areas of urban planning, environmental monitoring, and ecological restoration. Its unique segmented sampling strategy, which collects data from multiple angles, ensures accurate and reliable GVI measurements, which makes it especially suitable for decision-making support in complex urban environments.

In urban planning, public managers can utilize the GVC method to gain a detailed, comprehensive understanding of green space distribution across different regions. They can further identify both well-developed green zones and areas that need improvement by spatially evaluating the GVI. For example, the GVC method can be used to assess potential green spaces when planning new residential neighborhoods, which enables planners to promote healthier urban environments and improve residents' quality of life.

The GVC method also provides a valuable tool for the environmental monitoring and routine assessments of green spaces. By regularly tracking variations in the GVI, managers can swiftly identify areas in which vegetation health is deteriorating or in which new greening initiatives are needed. This facilitates timely interventions and a more proactive approach to managing urban ecosystems, ensuring that the city's green spaces contribute effectively to air quality, heat mitigation, and overall sustainability.

In ecological restoration projects, the GVC method allows for the more precise evaluation of vegetation recovery efforts. By assessing the GVI at different stages of restoration, managers can pinpoint areas that are responding well and those that may need adjustments. This enables the more effective fine-tuning of restoration strategies and resource allocation, ultimately enhancing the long-term success of ecological restoration projects.

Additionally, the GVC method can be applied in public spaces for real-time monitoring. For example, GVC electronic detection systems could be installed in urban parks and green spaces to continuously assess the health of urban vegetation. Similarly, GVC signage could be placed at pedestrian intersections to help residents identify the greenest routes and enhance their travel experience.

In conclusion, the spatial analysis capabilities of the GVC method are indispensable for the refined management of urban green spaces and provide a powerful tool for optimizing and sustaining the urban environment.

8. Conclusions

8.1. Key Findings

This study first provided a detailed theoretical exposition and applicability analysis of the six existing street view sampling methods, systematically evaluating their impact on the GVI calculations. Subsequently, we introduced a GVI calculation method based on three street view images and conducted a comprehensive comparative analysis of all the sampling methods. The experimental results demonstrate that this method achieved an effective balance between capturing greenery information and reducing computational costs, demonstrating high practicality and accuracy. The results also demonstrate the objective existence of errors.

Furthermore, to minimize errors, this study introduced a novel GVC concept by calculating the GVI corresponding to different initial angles and constructing a radar-like chart of the sampling points' GVI. The area of the GVC chart was used to represent the greening level of each point. The GVC method offers a new perspective for urban greening assessments and is well-suited to complex and diverse urban environments. By employing angular segment sampling, this method not only enhances the precision of GVI calculations but also significantly improves the consistency and reliability of the results. The potential value of this method for practical applications will facilitate future urban greening research.

8.2. Research Limitations

This study has certain limitations. First, we solely focused our study on a limited subset of street views in Hitachi City, Japan, resulting in a relatively small sample size. Second, we only used one tool for street-view GVI identification, thus neglecting the potential discrepancies that could arise when employing different identification tools. Additionally, although the 120° stitching method performed well in the experiments, its applicability across different urban and street view contexts requires further validation. Finally, the GVC method faces challenges related to data processing and computational complexity, which require further attention.

8.3. Future Research Directions

Future studies should expand the sample range and utilize multiple tools for street-view GVI identification to more comprehensively evaluate the applicability of various methods. Moreover, exploring innovative street-view sampling techniques could enhance the precision and broader applicability of GVI calculations. Such efforts would contribute to a deeper understanding and improve the practical use of this crucial urban environmental metric, thus offering more scientifically grounded insights for urban green space planning and management. Future research could leverage the precise spatial identification capabilities of the GVC method to analyze street greening and thereby assist in the design and implementation of optimized urban greening strategies.

Author Contributions: Conceptualization, D.Y. and T.H.; methodology, D.Y. and T.H.; software, D.Y.; validation, D.Y. and T.H.; formal analysis, D.Y.; investigation, D.Y.; resources, T.H.; data curation, D.Y.; writing—original draft preparation, D.Y.; writing—review and editing, T.H.; visualization, D.Y.; supervision, T.H.; project administration, T.H. All authors have read and agreed to the published version of the manuscript.

Funding: This research received no external funding.

Informed Consent Statement: Not applicable.

Data Availability Statement: The original data presented in the study are openly available. Publicly available data can be acquired through the links provided in the references.

Acknowledgments: This study was completed thanks to the AI GVI Survey Program provided by the Urban Planning Department, Urban Planning Division, Ministry of Land, Infrastructure, Transport and Tourism, National Institute for Land and Infrastructure management of Japan.

Conflicts of Interest: The authors declare no conflicts of interest.

References

1. Aoki, Y. Relationship between perceived greenery and width of visual fields. *J. Jpn. Inst. Landsc. Arch.* **1987**, *51*, 1–10. [CrossRef]
2. Toikka, A.; Willberg, E.; Mäkinen, V.; Toivonen, T.; Oksanen, J. The green view dataset for the capital of Finland, Helsinki. *Data Brief* **2020**, *30*, 105601. [CrossRef] [PubMed]
3. Dong, R.; Zhang, Y.; Zhao, J. How green are the streets within the sixth ring road of Beijing? An analysis based on tencent street view pictures and the green view index. *Int. J. Environ. Res. Public Health* **2018**, *15*, 1367. [CrossRef] [PubMed]
4. Yang, J.; Zhao, L.; Mcbride, J.; Gong, P. Can you see green? Assessing the visibility of urban forests in cities. *Landsc. Urban Plan.* **2009**, *91*, 97–104. [CrossRef]
5. Miao, S.; Xiao, Y. Exploring the spatial trade-off effects of green space on older people's physical inactivity: Evidence from Shanghai. *Landsc. Urban Plan.* **2024**, *251*, 105155. [CrossRef]
6. Wang, J.; Liu, W.; Gou, A. Numerical characteristics and spatial distribution of panoramic Street Green View index based on SegNet semantic segmentation in Savannah. *Urban For. Urban Green.* **2022**, *69*, 127488. [CrossRef]
7. Chen, S.; He, P.; Yu, B.; Wei, D.; Chen, Y. The challenge of noise pollution in high-density urban areas: Relationship between 2D/3D urban morphology and noise perception. *Build. Environ.* **2024**, *253*, 111313. [CrossRef]
8. Lin, J.; Wang, Q.; Huang, B. Street trees and crime: What characteristics of trees and streetscapes matter. *Urban For. Urban Green.* **2021**, *65*, 127366. [CrossRef]
9. Huang, D.; Kyttä, M.; Kajosaari, A.; Xie, X.; Zhang, J. One approach does not fit all settings: Exploring the effects of natural and built environments on running pleasantness across places. *Build. Environ.* **2023**, *245*, 110961. [CrossRef]
10. Chen, K.; Tian, M.; Zhang, J.; Xu, X.; Yuan, L. Evaluating the seasonal effects of building form and street view indicators on street-level land surface temperature using random forest regression. *Build. Environ.* **2023**, *245*, 110884. [CrossRef]
11. Dang, H.; Li, J. The integration of urban streetscapes provides the possibility to fully quantify the ecological landscape of urban green spaces: A case study of Xi'an city. *Ecol. Indic.* **2021**, *133*, 108388. [CrossRef]
12. Wang, B.; Xu, T.; Gao, H.; Ta, N.; Chai, Y.; Wu, J. Can daily mobility alleviate green inequality from living and working environments? *Landsc. Urban Plan.* **2021**, *214*, 104179. [CrossRef]
13. Zhu, J.; Qiu, L.; Su, Y.; Guo, Q.; Hu, T.; Bao, H.D.X.; Luo, J.; Wu, S.; Xu, Q.; Wang, Z.; et al. Disentangling the effects of the surrounding environment on street-side greenery: Evidence from Hangzhou. *Ecol. Indic.* **2022**, *143*, 109153. [CrossRef]

14. Tong, M.; She, J.; Tan, J.; Li, M.; Ge, R.; Gao, Y. Evaluating Street Greenery by Multiple Indicators Using Street-Level Imagery and Satellite Images: A Case Study in Nanjing, China. *Forests* **2020**, *11*, 1347. [CrossRef]
15. Li, X.; Zhang, C.; Li, W.; Ricard, R.; Meng, Q.; Zhang, W. Assessing street-level urban greenery using Google Street View and a modified green view index. *Urban For. Urban Green.* **2015**, *14*, 675–685. [CrossRef]
16. Biljecki, F.; Zhao, T.; Liang, X.; Hou, Y. Sensitivity of measuring the urban form and greenery using street-level imagery: A comparative study of approaches and visual perspectives. *Int. J. Appl. Earth Obs. Geoinf.* **2023**, *122*, 103385. [CrossRef]
17. Cui, Q.; Zhang, Y.; Yang, G.; Huang, Y.; Chen, Y. Analysing gender differences in the perceived safety from street view imagery. *Int. J. Appl. Earth Obs. Geoinf.* **2023**, *124*, 103537. [CrossRef]
18. View. Available online: https://dictionary.cambridge.org/us/dictionary/english/view (accessed on 21 January 2025).
19. Regus-Leidig, H.; Brandstätter, J.H. Structure and function of a complex sensory synapse. *Acta Physiol.* **2012**, *204*, 479–486. [CrossRef]
20. Livingstone, M. Vision and Art: The Biology of Seeing. *Nature* **2002**, *418*, 918–919. [CrossRef]
21. Smith, A. JOHANNES KEPLER, Optics. Paralipomena to Witelo & Optical Part of Astronomy. English translation by William H. Donahue. Sante Fe: Green Lion Press, 2000. Pp. xv+459. ISBN 1-888009-12-8. $55.00. *Br. J. Hist. Sci.* **2002**, *35*, 213–250. [CrossRef]
22. Tulving, E. Episodic Memory and Autonoesis: Uniquely Human? In *The Missing Link in Cognition: Origins of self-Reflective Consciousness*; Oxford University Press: Oxford, UK, 2005; pp. 3–56. [CrossRef]
23. Martins, D.M.; Manda, J.M.; Goard, M.J.; Parker, P.R.L. Building egocentric models of local space from retinal input. *Curr. Biol.* **2024**, *34*, R1185–R1202. [CrossRef] [PubMed]
24. Dey, A. Perceptual Characteristics of Visualizations for Occluded Objects in Handheld Augmented Reality. Ph.D. Thesis, University of South Australia, Adelaide, Australia, 2013.
25. Biljecki, F.; Ito, K. Street view imagery in urban analytics and GIS: A review. *Landsc. Urban Plan.* **2021**, *215*, 104217. [CrossRef]
26. Bourke, P.D. Synthetic Stereoscopic Panoramic Images. In Proceedings of the International Conference on Virtual Systems and MultiMedia, Xi'an, China, 18–20 October 2006.
27. Gilge, C.R. Google Street View and the Image as Experience. *GeoHumanities* **2016**, *2*, 469–484. [CrossRef]
28. Li, L.; Yao, J.; Xie, R.; Xia, M.; Zhang, W. A Unified Framework for Street-View Panorama Stitching. *Sensors* **2017**, *17*, 1. [CrossRef] [PubMed]
29. Museum of GIS Technology. Available online: http://mogist.kkc.co.jp/word/40ed3667-af74-4cc0-b89a-546e02f34f1f.html (accessed on 10 December 2024).
30. Kyoto City: "Kyoto City Green Master Plan" [2010–2025]. Available online: https://www.city.kyoto.lg.jp/kensetu/page/0000077122.html (accessed on 10 December 2024).
31. New Osaka City Green Master Plan Formulated (...Master Plan of> Afforestation >Osaka City Green). Available online: https://www.city.osaka.lg.jp/kensetsu/page/0000239835.html (accessed on 10 December 2024).
32. Shinjuku City Green Master Plan: Shinjuku City. Available online: https://www.city.shinjuku.lg.jp/seikatsu/file14_04_00001.html (accessed on 10 December 2024).
33. Detailed Control Plan for the Capital Functional Core Area (Block Level) (2018–2035)_Municipal Detailed Plan_Beijing Municipal Planning and Natural Resources Commission. Available online: https://ghzrzyw.beijing.gov.cn/zhengwuxinxi/ghcg/xxgh/sj/202008/t20200829_1993379.html (accessed on 10 December 2024).
34. *DB11/T 1877-2021*; Technical Specification of Ecological and Environmental Quality Evaluation. Beijing Municipal Administration for Market Regulation: Beijing, China, 2021.
35. Notice of the General Office of the Guangzhou Municipal People's Government on the issuance of the Guangzhou Green Space System Plan (2021–2035). Available online: https://www.gz.gov.cn/gkmlpt/content/9/9224/post_9224694.html#12624 (accessed on 10 December 2024).
36. Notice of the Shenzhen Municipal People's Government on Issuing the Shenzhen Park City Construction Master Plan and Three-Year Action Plan (2022–2024). Available online: https://www.sz.gov.cn/zfgb/2023/gb1272/content/post_10389162.html (accessed on 10 December 2024).
37. Seoul Solution. Available online: https://www.seoulsolution.kr/en/content/2030-seoul-plan (accessed on 10 December 2024).
38. Ki, D.; Kim, S.; Lee, S. Analysis of the Green Equity Using Google Street View and Deep Learning in Seoul, Korea: Focused on the Comparison between NDVI and Street Image-Based Green Calculation Method. *J. Korea Plan. Assoc.* **2021**, *56*, 194–211. [CrossRef]
39. Google Maps Platform | Google for Developers. Available online: https://developers.google.com/maps (accessed on 16 June 2024).
40. Treepedia:: MIT Senseable City Lab. Available online: http://senseable.mit.edu/treepedia (accessed on 10 December 2024).
41. Hu, K.; Zhang, Z.; Li, Y.; Wang, S.; Ye, T.; Song, J.; Zhang, Y.; Wei, J.; Cheng, J.; Shen, Y. Urban overall and visible greenness and diabetes among older adults in China. *Landsc. Urban Plan.* **2023**, *240*, 104881. [CrossRef]
42. Pan, J.; Hu, K.; Yu, X.; Li, W.; Shen, Y.; Song, Z.; Guo, Y.; Yang, M.; Hu, F.; Xia, Q. Beneficial associations between outdoor visible greenness at the workplace and metabolic syndrome in Chinese adults. *Environ. Int.* **2024**, *183*, 108327. [CrossRef]

43. Xiao, Y.; Zhang, Y.; Sun, Y.; Tao, P.; Kuang, X. Does green space really matter for residents' obesity? A new perspective from Baidu street view. *Front. Public Health* **2020**, *8*, 332. [CrossRef]
44. Yu, H.; Zhou, Y.; Wang, R.; Qian, Z.; Knibbs, L.D.; Jalaludin, B.; Schootman, M.; McMillin, S.E.; Howard, S.W.; Lin, L.-Z. Associations between trees and grass presence with childhood asthma prevalence using deep learning image segmentation and a novel green view index. *Environ. Pollut.* **2021**, *286*, 117582. [CrossRef]
45. Yu, H.; Hu, L.-W.; Zhou, Y.; Qian, Z.; Schootman, M.; LeBaige, M.H.; Zhou, Y.; Xiong, S.; Shen, X.; Lin, L.-Z. Association between eye-level greenness and lung function in urban Chinese children. *Environ. Res.* **2021**, *202*, 111641. [CrossRef]
46. Liu, Y.; Pan, X.; Liu, Q.; Li, G. Establishing a reliable assessment of the green view index based on image classification techniques, estimation, and a hypothesis testing route. *Land* **2023**, *12*, 1030. [CrossRef]
47. Yu, X.; Zhao, G.; Chang, C.; Yuan, X.; Heng, F. Bgvi: A new index to estimate street-side greenery using baidu street view image. *Forests* **2018**, *10*, 3. [CrossRef]
48. Zhang, W.; Zeng, H. Spatial differentiation characteristics and influencing factors of the green view index in urban areas based on street view images: A case study of Futian District, Shenzhen, China. *Urban For. Urban Green.* **2024**, *93*, 128219. [CrossRef]
49. Liu, Y.; Li, Y.; Yang, W.; Hu, J. Exploring nonlinear effects of built environment on jogging behavior using random forest. *Appl. Geogr.* **2023**, *156*, 102990. [CrossRef]
50. Yang, W.; Chen, H.; Li, J.; Guo, W.; Fei, J.; Li, Y.; He, J. How does visual environment affect outdoor jogging behavior? Insights from large-scale city images and GPS trajectories. *Urban For. Urban Green.* **2024**, *95*, 128291. [CrossRef]
51. Yang, W.; Hu, J.; Liu, Y.; Guo, W. Examining the influence of neighborhood and street-level built environment on fitness jogging in Chengdu, China: A massive GPS trajectory data analysis. *J. Transp. Geogr.* **2023**, *108*, 103575. [CrossRef]
52. Huang, Z.; Tang, L.; Qiao, P.; He, J.; Su, H. Socioecological justice in urban street greenery based on green view index-A case study within the Fuzhou Third Ring Road. *Urban For. Urban Green.* **2024**, *95*, 128313. [CrossRef]
53. Yutian, L.; Running, C.; Bin, C.; Jiayu, W. Inclusive green environment for all? An investigation of spatial access equity of urban green space and associated socioeconomic drivers in China. *Landsc. Urban Plan.* **2024**, *241*, 104926. [CrossRef]
54. Zhang, J.; Hu, A. Analyzing green view index and green view index best path using Google street view and deep learning. *J. Comput. Des. Eng.* **2022**, *9*, 2010–2023. [CrossRef]
55. Huang, D.; Jiang, B.; Yuan, L. Analyzing the effects of nature exposure on perceived satisfaction with running routes: An activity path-based measure approach. *Urban For. Urban Green.* **2022**, *68*, 127480. [CrossRef]
56. Liang, C.; Jiang, H.; Yang, S.; Tian, P.; Ma, X.; Tang, Z.; Wang, H.; Wang, W. Characterizing street trees in three metropolises of central China by using Street View data: From individual trees to landscape mapping. *Ecol. Inform.* **2024**, *80*, 102480. [CrossRef]
57. Qi, L.; Hu, Y.; Bu, R.; Xiong, Z.; Li, B.; Zhang, C.; Liu, H.; Li, C. Spatial-temporal patterns and influencing factors of the Building Green View Index: A new approach for quantifying 3D urban greenery visibility. *Sustain. Cities Soc.* **2024**, *111*, 105518. [CrossRef]
58. Tang, J.-H.; Huang, Y.-J.; Lee, P.-H.; Lee, Y.-T.; Wang, Y.-C.; Chan, T.-C. Associations between community green view index and fine particulate matter from Airboxes. *Sci. Total Environ.* **2024**, *921*, 171213. [CrossRef]
59. Puppala, H.; Tamvada, J.P.; Kim, B.; Peddinti, P.R. Enhanced green view index. *MethodsX* **2022**, *9*, 101824. [CrossRef] [PubMed]
60. Chen, J.; Zhou, C.; Li, F. Quantifying the green view indicator for assessing urban greening quality: An analysis based on Internet-crawling street view data. *Ecol. Indic.* **2020**, *113*, 106192. [CrossRef]
61. Chen, Y.; Zhang, Q.; Deng, Z.; Fan, X.; Xu, Z.; Kang, X.; Pan, K.; Guo, Z. Research on Green View Index of Urban Roads Based on Street View Image Recognition: A Case Study of Changsha Downtown Areas. *Sustainability* **2022**, *14*, 16063. [CrossRef]
62. Tsai, V.J.; Chang, C.T. Three-dimensional positioning from Google street view panoramas. *IET Image Process.* **2013**, *7*, 229–239. [CrossRef]
63. Ki, D.; Lee, S. Analyzing the effects of Green View Index of neighborhood streets on walking time using Google Street View and deep learning. *Landsc. Urban Plan.* **2021**, *205*, 103920. [CrossRef]
64. Yin, L.; Wang, Z. Measuring visual enclosure for street walkability: Using machine learning algorithms and Google Street View imagery. *Appl. Geogr.* **2016**, *76*, 147–153. [CrossRef]
65. Li, J.; Zhang, X.; Li, L.; Wang, X.; Cheng, J.; Gao, C.; Ling, J. An estimation method for multidimensional urban street walkability based on panoramic semantic segmentation and domain adaptation. *Eng. Appl. Artif. Intell.* **2024**, *136*, 108905. [CrossRef]
66. Huang, C.; Hu, T.; Duan, Y.; Li, Q.; Chen, N.; Wang, Q.; Zhou, M.; Rao, P. Effect of urban morphology on air pollution distribution in high-density urban blocks based on mobile monitoring and machine learning. *Build. Environ.* **2022**, *219*, 109173. [CrossRef]
67. Hu, Y.; Qian, F.; Yan, H.; Middel, A.; Wu, R.; Zhu, M.; Han, Q.; Zhao, K.; Wang, H.; Shao, F. Which street is hotter? Street morphology may hold clues-thermal environment mapping based on street view imagery. *Build. Environ.* **2024**, *262*, 111838. [CrossRef]
68. Zhang, S.; Yuan, C.; Ma, B.; Liu, N.; Li, W. Coupling effects of building-vegetation-land on seasonal land surface temperature on street-level: A study from a campus in Beijing. *Build. Environ.* **2024**, *262*, 111790. [CrossRef]
69. Sevtsuk, A.; Basu, R.; Li, X.; Kalvo, R. A big data approach to understanding pedestrian route choice preferences: Evidence from San Francisco. *Travel Behav. Soc.* **2021**, *25*, 41–51. [CrossRef]

70. Qiu, W.; Zhang, Z.; Liu, X.; Li, W.; Li, X.; Xu, X.; Huang, X. Subjective or objective measures of street environment, which are more effective in explaining housing prices? *Landsc. Urban Plan.* **2022**, *221*, 104358. [CrossRef]
71. Xu, Y.; Qi, C.; Feng, H.; Niu, Y. Research on the Exploration and Algorithm on Dynamic Visible Green Index Model. *Urban Dev. Stud.* **2022**, *29*, 22–28.
72. Human Eye. Available online: https://en.wikipedia.org/w/index.php?title=Human_eye&oldid=1270413881 (accessed on 22 January 2025).
73. Hitachi, Ibaraki. Available online: https://en.wikipedia.org/w/index.php?title=Hitachi,_Ibaraki&oldid=1267581805 (accessed on 22 January 2025).
74. OpenStreetMap. Available online: https://en.wikipedia.org/w/index.php?title=OpenStreetMap&oldid=1240279893 (accessed on 4 May 2024).
75. Kim, J.H.; Lee, S.; Hipp, J.R.; Ki, D. Decoding urban landscapes: Google street view and measurement sensitivity. *Comput. Environ. Urban Syst.* **2021**, *88*, 101626. [CrossRef]
76. Badrinarayanan, V.; Kendall, A.; SegNet, R.C. A deep convolutional encoder-decoder architecture for image segmentation. *arXiv* **2015**. [CrossRef]
77. Fu, G.; Liu, C.; Zhou, R.; Sun, T.; Zhang, Q. Classification for high resolution remote sensing imagery using a fully convolutional network. *Remote Sens.* **2017**, *9*, 498. [CrossRef]
78. Chen, F.-C. Back-propagation neural networks for nonlinear self-tuning adaptive control. *IEEE Control Syst. Mag.* **1990**, *10*, 44–48. [CrossRef]
79. Chen, L.-C.; Papandreou, G.; Kokkinos, I.; Murphy, K.; Yuille, A.L. Deeplab: Semantic image segmentation with deep convolutional nets, atrous convolution, and fully connected crfs. *IEEE Trans. Pattern Anal. Mach. Intell.* **2017**, *40*, 834–848. [CrossRef] [PubMed]
80. Recent Research | Urban Research Department Urban Development Laboratory. Available online: https://www.nilim.go.jp/lab/jeg/current-fields.html (accessed on 10 December 2024).
81. Howard, A.; Sandler, M.; Chu, G.; Chen, L.-C.; Chen, B.; Tan, M.; Wang, W.; Zhu, Y.; Pang, R.; Vasudevan, V.; et al. Searching for MobileNetV3. *arXiv* **2019**, arXiv:1905.02244.
82. de la Iglesia Martinez, A.; Labib, S.M. Demystifying normalized difference vegetation index (NDVI) for greenness exposure assessments and policy interventions in urban greening. *Environ. Res.* **2023**, *220*, 115155. [CrossRef] [PubMed]
83. Bai, Z.; Wang, Z.; Li, D.; Wang, X.; Jian, Y. The relationships between 2D and 3D green index altered by spatial attributes at high spatial resolution. *Urban For. Urban Green.* **2024**, *101*, 128540. [CrossRef]
84. Su, L.; Chen, W.; Zhou, Y.; Fan, L.; Li, J. Exploring Urban Street Green Perception from the Perspective of Combining GVI and NDVI: A Case Study of Zhongshan City, Guangdong Province. *bioRxiv* **2023**. [CrossRef]
85. Hao, X.; Long, Y. Street Greenery: A New Indicator for Evaluating Walkability. *Shanghai Urban Plan. Rev.* **2017**, *1*, 32–36.